Hindawi

Research Article

Pansharpening with the Multidirection Tree Ridgelet Dictionary

Hong Li [ID], Gaining Han, Zongsheng Wu, and Xiaoxue Song

School of Computer Science, Xianyang Normal University, Xianyang 712000, China

Correspondence should be addressed to Hong Li; honglishining@163.com

In this work, we propose a novel pansharpening method based on the multidirection tree ridgelet dictionary. A pansharpened image has a wide-ranging application area, such as object detection, image segmentation, feature extraction, and so on. Remote sensing (RS) imagery contains more abundant information on surface features. In order to represent different object information, we use three main classes of different dictionaries, which can reveal the latent structure of RS image. First, RS imagery is divided into several blocks. Each block is classified as smooth, irregular, or multidirection categories. Different categories are sparsely represented in different dictionaries. Second, the smooth blocks are sparsely represented in the discrete cosine transform (DCT) dictionary. The irregular and the multidirection blocks are sparsely represented in the KSVD and multidirection tree ridgelet (MDTR) dictionary, respectively. Finally, we can obtain the fusion image by reconstructing those blocks. Some experiments are taken on three different datasets acquired by QuickBird, GeoEye, and IKONOS satellites. Experimental results show that the proposed method can reduce spectral distortion and enhance spatial information. Meanwhile, numerical guidelines outperform some related methods.

1. Introduction

Pansharpening refers to the fusion of a panchromatic (PAN) image and a multispectral (MS) or hyperspectral (HS) image. PAN has high spatial resolution but low spectral resolution. MS or HS has high spectral resolution but low spatial resolution. The fused imagery, which is unachievable by a single sensor, has not only high spatial resolution but also high spectral resolution, and the fused image can protect more detailed information for the downstream object detection, image segmentation, and feature extraction. Many fusion measures have been proposed. Generally, these measures can be divided into four main categories [1].

(1) Component substitution-based (CS) methods [2–4]

(2) Multiscale analysis-based (MRA) methods [5, 6]

(3) Degradation model-based (DM) methods [7–17]

(4) Deep neural network-based (DNN) methods [18–21]

CS methods include principal component analysis (PCA) and intensity-hue-saturation (IHS). CS methods behave well in computational efficiency. Due to the spectral discrepancies between the cover ranges of MS and PAN images, the spectral distortions usually can be found in the fused image. For the MRA category, the missing spatial information of MS image can be extracted from the PAN image via multiscale analysis tools. However, these methods can raise spatial artifacts.

In the DM category, image fusion is the degradation problem. These methods require additional priors to regularize the solution space. Li and Yang [7] proposed a new fusion method based on compressed sensing, which used the MS and PAN images through a KSVD [22] dictionary. Zhu and Bamler proposed the SparseFI method [8]. In SparseFI method, the atoms of coupling dictionaries came from the PAN image. In Ref. [9], the PN-TSSC method was proposed followed by SparseFI, and the PN-TSSC method was a two-step sparse coding method. In the study in Ref. [10], the reconstruction of the fusion imagery was achieved by using the identical sparse representation coefficients on the coupling dictionaries. Wang et al. [11] proposed a novel hybrid dictionary to fuse the RS imagery. However, those above methods had ignored the internal structural diversity information of RS imagery. Li et al. [12] proposed a novel

pansharpening method with NSCT and HSAE, in which the detailed information was hierarchically injected into the MS image. In Ref. [13], Zhang et al. put forward a new RS fusion method, in which multiscale convolution sparse decomposition was used to extract more subtle feature. The similarity is important information in image processing. Thus, pansharpening based on similarity was proposed [14–16]. Li et al. [14] proposed a local geometrical similarity-based method to capture detailed information. In Ref. [15], the similarity was obtained by a local adaptive sparse representation metric. Zhang et al. [16] proposed a spatial weighted neighborhood embedding method sharing the similar manifold structure. Nonnegative matrix factorization is a noteworthy method in RS image fusion. Nonnegativity is also used to reduce the ill-posedness of the spectral and spatial degradation models. In Ref. [17], semi-NMF based pansharpening was proposed to improve the image effect. DM methods enhance the image quality; however, the complexity is high for these methods.

Recently, the DNN methods are arousing more attention. In Ref. [18], the salient features can be extracted through two branches DNNs. The image feature, extracted from the convolutional layers, yielded the fusion result. In Ref. [19], the Pan-GAN model was proposed, and this method did not rely on the ground truth. Zhang et al. [20] proposed an SSE network-based pansharpening. In this paper, AFFMs were used to merge image features through information content. NLRNet was proposed for RS image fusion [21]. The author proposed the ENLA mechanism and ReZero technology to spread the signal easily, and the SpecAM was used to adjust the spectral information. However, DNN methods show that the training time is long and the sample size is large.

RS image contains various types of ground objects. Multiscale analysis tools have been used to capture image orientation information, and researchers have also demonstrated their excellent performance in processing geometric information. Based on this, we propose a novel pansharpening with a multidirection tree ridgelet dictionary to represent the diverse information of RS image. First, RS imagery is divided into several blocks. Each block is classified as smooth, irregular, or multidirection categories. Different categories are sparsely represented in different dictionaries. Second, we construct the discrete cosine transform (DCT), KSVD, and multidirection tree ridgelet (MDTR) dictionaries. Smooth and irregular blocks are sparsely represented in DCT and KSVD dictionaries, respectively, and the direction blocks are sparsely represented in the MDTR dictionary.

The contribution of this work is as follows: (1) the multidirection ridgelet dictionary can be constructed via discretized parameters of ridgelet function; (2) spatial details can be captured by sparsely encoding patches in DCT, KSVD, or MDTR dictionaries. The proposed approach has performed three different datasets acquired by the QuickBird, GeoEye, and IKONOS. The experimental results show that the proposed MDTR method can outperform its counterparts.

The remainder of this paper is structured as follows. The construction of the MDTR dictionary is depicted in Section 2. Section 3 presents the pansharpening method by taking the MDTR dictionary. Some experiments on different datasets are performed in Section 4. Finally, Section 5 concisely reviews conclusions.

2. Construction of the Multidirection Tree Ridgelet Dictionary

One of the major problems in sparse representation is the construction of dictionary. In view of the inherent diversity of RS image and other characteristics, in our paper, we construct three different dictionaries, namely, DCT [12], KSVD [22], and MDTR dictionaries. The DCT dictionary can represent the smooth region. The KSVD dictionary is used to learn the information of the irregular blocks adaptively. The MDTR dictionary is used to sparsely represent direction blocks.

Ridgelet scale function is

$$\psi_\gamma(x) = a^{-1/2} \psi\left(\frac{(x_1 \cos\theta + x_2 \sin\theta - b)}{a}\right), \qquad (1)$$

where $x = (x_1, x_2)^T \in R^2$ and $\psi(x) = e^{-x^2/2} - 1/2e^{-x^2/8}$.

The prototype of the ridgelet dictionary is

$$\psi_\gamma(x) = K_{(\gamma)}\left(e^{-x^2/2} - \frac{1}{2}e^{-x^2/8}\right), \qquad (2)$$

where $x = a(x_1 \cos\theta + x_2 \sin\theta - b)$, $K_{(\gamma)}$ is a normalized factor, $\gamma = (a, b, \theta)$, a is the scale parameter, b is the location parameter, and θ is the direction parameter.

We can obtain the ridgelet dictionary via discretization of a, b, and θ. Figure 1 shows the ridgelet function with different parameters. Figure 1(a) is the ridgelet function. And Figures 1(b)–1(e) are the result of different parameters.

The ridgelet dictionary can be obtained by discretized three parameters (a, b, and θ). Lin et al. [23] proposed the collaborative compressed sensing reconstruction method. Authors proposed that the natural images were reconstructed by using the overcomplete ridgelet dictionary. It can be seen that the overcomplete ridgelet dictionary shows its advantages in image processing, which can maintain the structure and edge information of the image. However, the large-scale overcomplete ridgelet dictionary increases the complexity of the algorithm. In our work, we propose a novel fusion method with the multidirection tree ridgelet dictionary. The multidirection tree ridgelet dictionary shows superior fusion results than the global ridgelet dictionary and requires less time complexity. Figure 2 shows ridgelet dictionaries. Figure 2(a) represents the global ridgelet dictionary. Figures 2(b)–2(f) are the different direction ridgelet dictionaries, respectively.

3. Image Fusion Using the Multidirection Tree Ridgelet Dictionary

In order to represent the structural diversity, image blocks are classified into different categories, e.g., smooth category, irregular category, or multidirection category. Figure 3 shows the classification results of blocks. Figure 3(a) shows a PAN image. Figures 3(b)–3(h) show the blocks
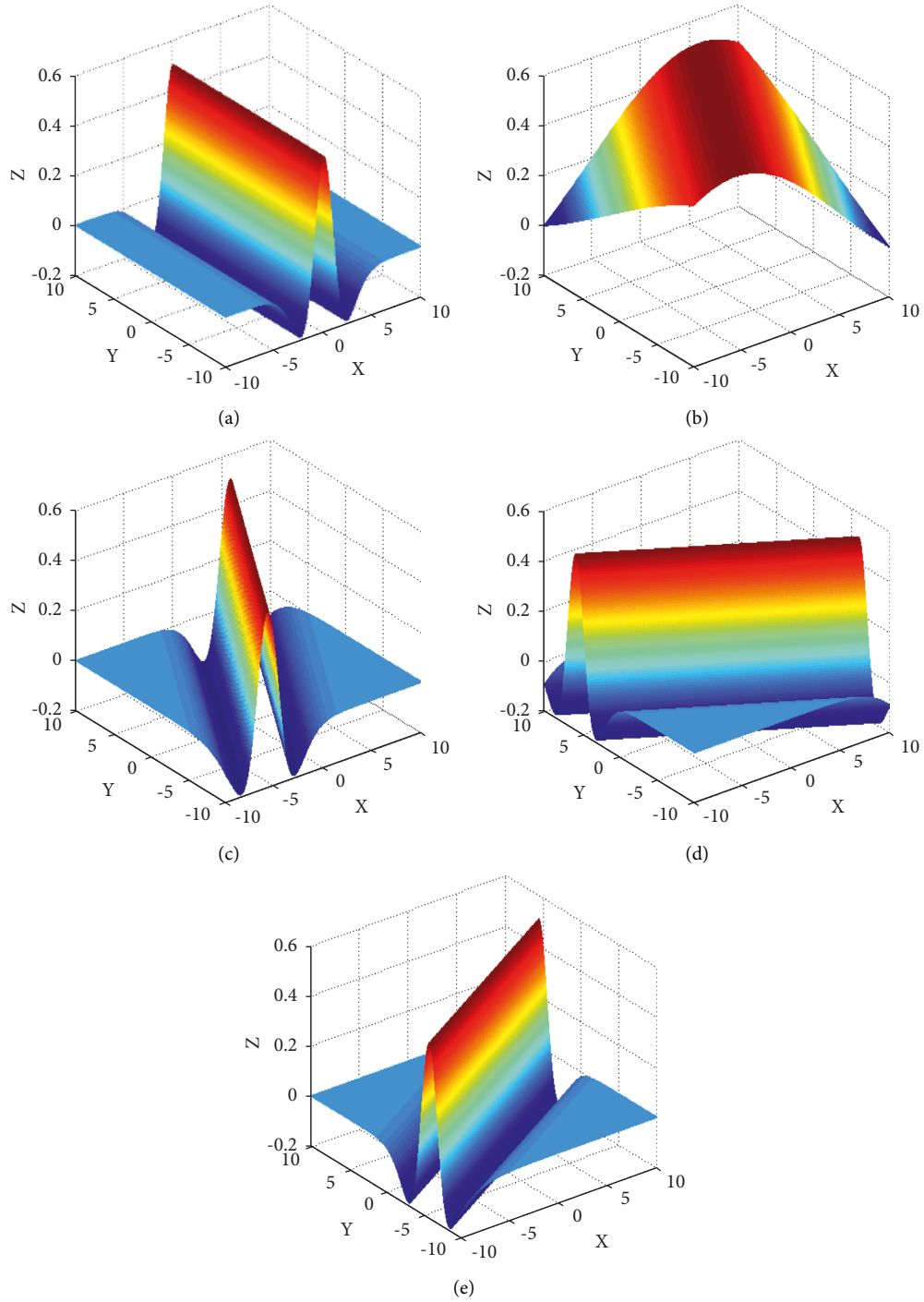
FIGURE 1: Ridgelet function. (a) Ridgelet function. (b) $a = 0.1$. (c) $a = 1$. (d) $\theta = 60^0$. (e) $\theta = 120^0$.

of the PAN image. Figures 3(b)–3(c) show smooth and irregular blocks, respcetively. Figures 3(d)–3(h) are direction blocks.

3.1. Smooth Category. Set the threshold, $Thres_1$. Calculate the variance, std, of each block. If the variance is less than the threshold ($std < Thres_1$), then the block is classified into the smooth category. For smooth blocks, the DCT dictionary, $\mathbf{D}_{DCT}$, is used for sparse representation.

3.2. Irregular Category. For each pixel of a block, we calculate the gradient in x and y direction. Then the gradient can be defined as

$$g_i = [\partial t'(x, y)/\partial x , \partial t'(x, y)/\partial y]. \tag{3}$$

The gradient matrix is indicated as $\mathbf{Grad}$ ($\mathbf{Grad} \in R^{n \times 2}$, $\mathbf{Grad} = [g_1, g_2, \ldots g_n]^{\mathbf{T}}$). Then, the gradient matrix is decomposed by singular value decomposition:
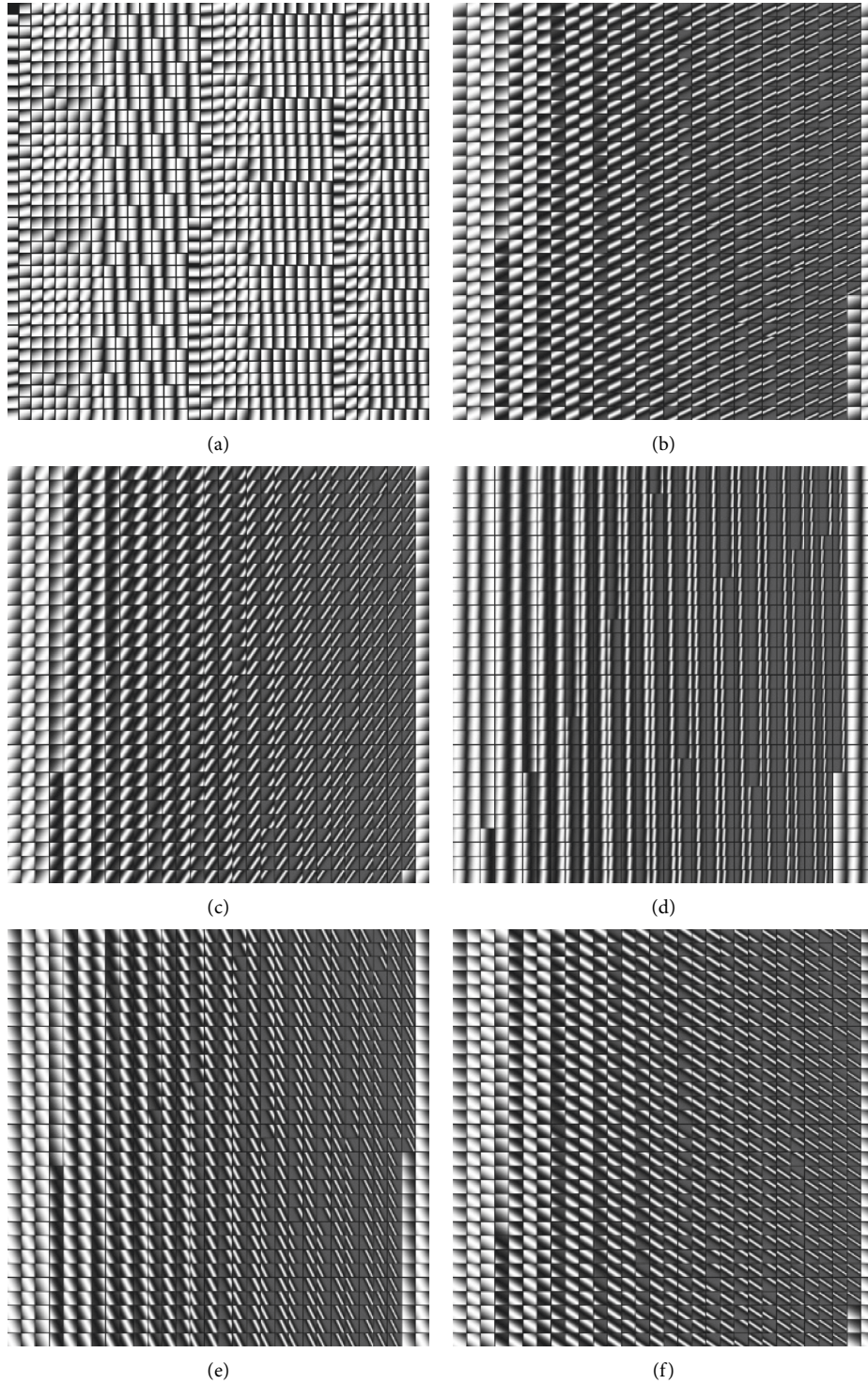
Figure 2: Ridgelet dictionary. (a) Global ridgelet dictionary. (b) MDTR dictionary ($\theta = 30^{\mathbf{o}}$). (c) MDTR dictionary ($\theta = 60^0$). (d) MDTR dictionary ($\theta = 90^0$). (e) MDTR dictionary ($\theta = 120^0$). (f) MDTR dictionary ($\theta = 150^0$).

$$\mathbf{Grad} = \mathbf{USV^T}. \tag{4}$$

R can be calculated as

$$R = \frac{S_{1,1} - S_{2,2}}{S_{1,1} + S_{2,2}}. \tag{5}$$

Set the threshold, Thres_2. If $R < \text{Thres}_2$, then the block is classified as the irregular category. Otherwise, the block can be considered multidirection category. For irregular blocks, the KSVD dictionary ($\mathbf{D}_{KSVD}$) is used for sparse reconstruction.
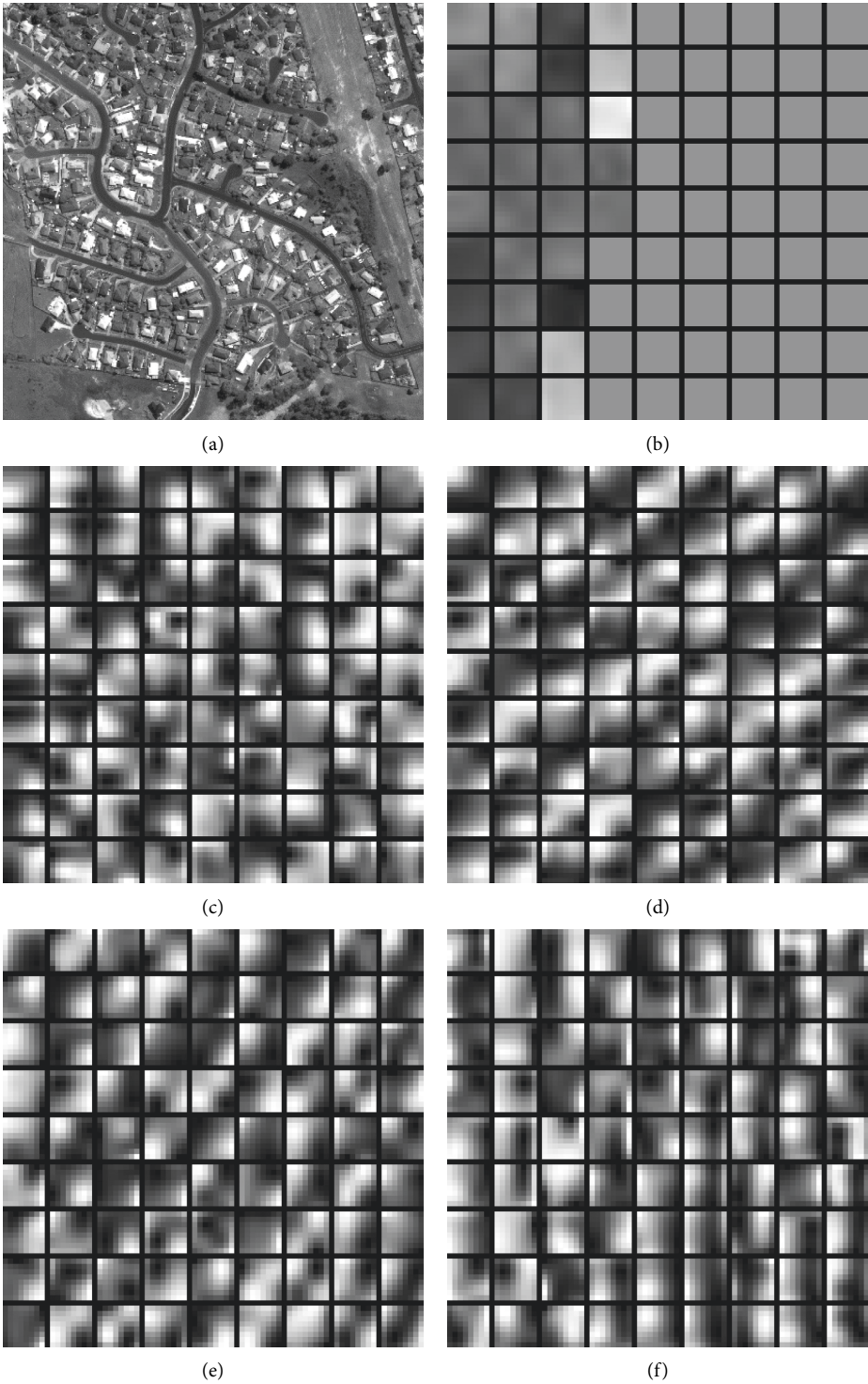
(a)

(b)

(c)

(d)
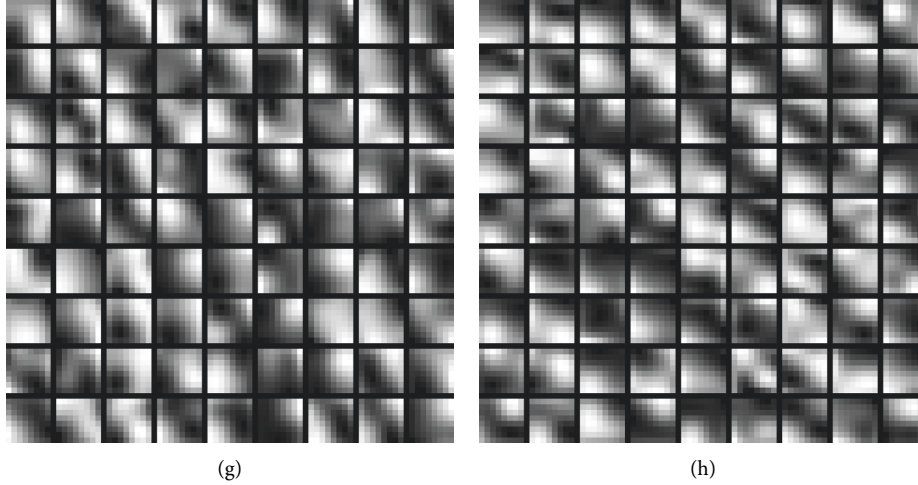

(e)

(f)

Figure 3: Continued.

(g)   (h)

Figure 3: Classification results of blocks. (a) PAN image. (b) Smooth blocks. (c) Irregular blocks. (d) Direction blocks ($\theta = 30^0$). (e) Direction blocks ($\theta = 60^0$). (f) Direction blocks ($\theta = 90^0$). (g) Direction blocks ($\theta = 120^0$). (h) Direction blocks ($\theta = 150^0$).

---

input: **the MS image $\overline{Y}_{MS}$ and the PAN image $\overline{Y}_{Pan}$**
output: **the fused MS image Y_{HMS}**
Step1: the first principal component $\mathbf{Y}_{PC1}$ of the resampled $\overline{Y}_{MS}$ and the $\overline{Y}_{Pan}$ were partitioned into blocks. Thus, we can obtain the $\{h_{pc1}^t\}_{t=1}^{num}$ and $\{h_{pan}^t\}_{t=1}^{num}$. *num* represents the number of blocks.
Step2: $\{h_{pan}^t\}_{t=1}^{num}$ are classified through the measure of section 3, which are divided into smooth, irregular, or multidirection categories. Correspondingly, $\{h_{pc1}^t\}_{t=1}^{num}$ is marked in the same category according to the classification of $\{h_{pan}^t\}_{t=1}^{num}$.
Step3: $\mathbf{D}_{DCT}$ and $\mathbf{D}_{KSVD}$ are used to smooth blocks and irregular blocks, respectively. According to the angle of image block, $\mathbf{D}_{Rig}^n$ is selected for multidirection category.
Step4: Finally, the fused block is obtained by sparse coding. Thus, $\mathbf{Y}_{HMS}$ can be obtained.

Algorithm 1: Pansharpening with multidirection tree ridgelet dictionary.

3.3. Multidirection Category.

In equation (4), the first column (v_1) of the matrix V is named as the first principal direction. The second column (v_2) of the matrix $\mathbf{V}$ is the second principal direction. The angle of the block is determined as

$$\theta = \arctan\left(\frac{v_1(2)}{v_2(1)}\right). \quad (6)$$

The MDTR dictionary is represented as $\mathbf{D}_{Rig}^n$, where $n(n = 1, \ldots, 18)$ is the number of $\mathbf{D}_{Rig}^n$. The angle range is set as $[0^0, 180^0]$; that is to say, there are 18 groups ridgelet dictionaries, and the interval of each group is 10^0. The angle of $\mathbf{D}_{Rig}^1$ is from 0^0 to 10^0. The angle of $\mathbf{D}_{Rig}^2$ is from 11^0 to 20^0. The angle of $\mathbf{D}_{Rig}^3$ is from 21^0 to 30^0 and so forth. For multidirection blocks, $\mathbf{D}_{Rig}^n$ is used for sparse reconstruction.

The fusion method is summarized in Algorithm 1.

4. Experimental Results

Three different datasets demonstrate the effectiveness of the proposed algorithm. The experimental results are compared with six related methods, which are the PCA method [2], GIHS method [3], CT method [5], SparseFI method [8], PN-TSSC method [9], and NMF method [17]. The parameters of each method are set according to the papers. The size of $\mathbf{D}_{DCT}$ and $\mathbf{D}_{KSVD}$ is 256 and 1024, respectively. There are 18 groups ridgelet dictionaries, and the interval of each group is 10^0. The objective quality evaluation indexes include CC [24], UIQI [25], RMSE, Q_4 [26], SAM [24], and ERGAS [24]. The best results is highlighted in bold. Table 1 shows the quality evaluation indexes.

4.1. QuickBird Dataset.

QuickBird has been acquired in Xi'an, China. The resolution is 0.61 m for the PAN image and 2.44 m for the MS image. Figure 4 shows all the fused results. Figures 4(a)–4(c) are MS, PAN, and reference MS images, respectively. Figures 4(d)–4(j) are the results obtained by employing the seven different fusion methods. In Figures 4(d)–4(j), the first row is the fused image, and the second row is the difference image between the fused image and reference image. In addition, we display the magnified area for each fused image.

We can see that the spatial information is improved for all the fused images. The fusion result of the PCA method is darkness. For the difference image, we can see that the result of CT is better than the result of GIHS. For the magnified

Table 1: The quality evaluation indexes.

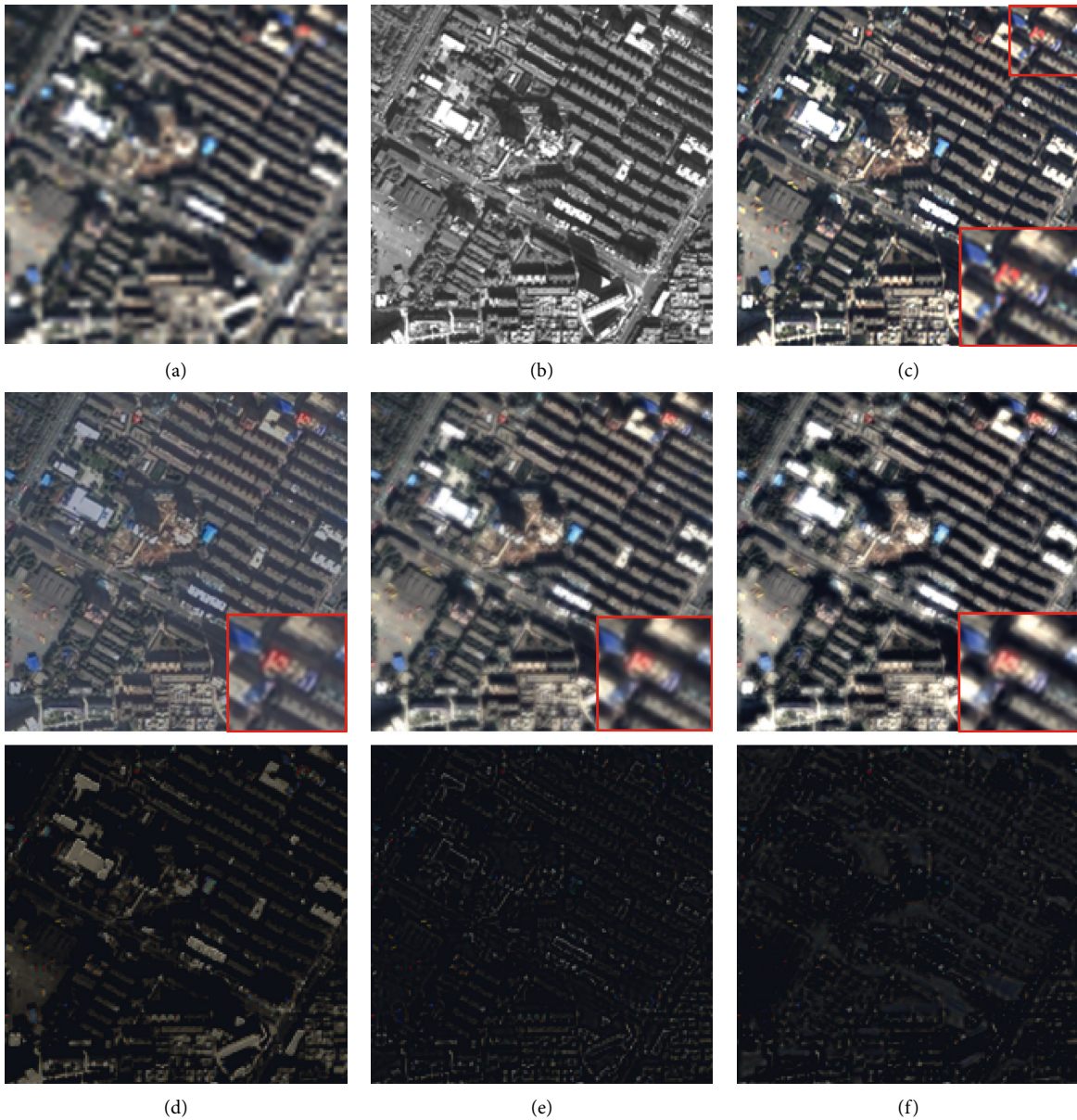| Index	Formula
CC	$CC = \dfrac{\sum_{i=1}^{M}\sum_{j=1}^{N}[\mathbf{F}_{(i,j)}-\mu_F][\mathbf{X}_{(i,j)}-\mu_X]}{\sqrt{\sum_{i=1}^{M}\sum_{j=1}^{N}[\mathbf{F}_{(i,j)}-\mu_F]^2\sum_{i=1}^{M}\sum_{j=1}^{N}[\mathbf{X}_{(i,j)}-\mu_X]^2}}$
UIQI	$UIQI = (\sigma_{FX}/(\sigma_F\sigma_X)) \times (2\mu_F\mu_X/(\mu_F^2+\mu_X^2)) \times (2\sigma_F\sigma_X/(\sigma_F^2+\sigma_X^2))$
RMSE	$RMSE = 1/MN\sqrt{\sum_{i=1}^{M}\sum_{j=1}^{N}[\mathbf{F}_{(i,j)}-\mathbf{X}_{(i,j)}]}$
Q_4	$Q_4 = E(\|Q4_{D\times D}\|)$ $Q4_{D\times D} = ((4[E(x\cdot y*)-\overline{x}\cdot\overline{y}*])/(E(\|x\|^2)-\|\overline{x}\|^2+E(\|y\|^2)-\|\overline{y}\|^2))\cdot((\|\overline{x}\|\cdot\|\overline{y}\|)/(\|\overline{x}\|^2+\|\overline{y}\|^2))$ $x = \mathbf{X}_1(\mathbf{i},\mathbf{j})+\alpha\mathbf{X}_2(\mathbf{i},\mathbf{j})+\beta\mathbf{X}_3(\mathbf{i},\mathbf{j})+\gamma\mathbf{X}_4(\mathbf{i},\mathbf{j})$ $y = \mathbf{F}_1(\mathbf{i},\mathbf{j})+\alpha\mathbf{F}_2(\mathbf{i},\mathbf{j})+\beta\mathbf{F}_3(\mathbf{i},\mathbf{j})+\gamma\mathbf{F}_4(\mathbf{i},\mathbf{j})$
SAM	$SAM = \arccos(\langle u_X, u_F\rangle/\|u_X\|_2.\|u_F\|_2)$
ERGAS	$ERGAS = 100\dfrac{h}{l}\sqrt{1/k\sum_{k=1}^{K}(RMSE/\mu_k)^2}$

(a)

(b)

(c)
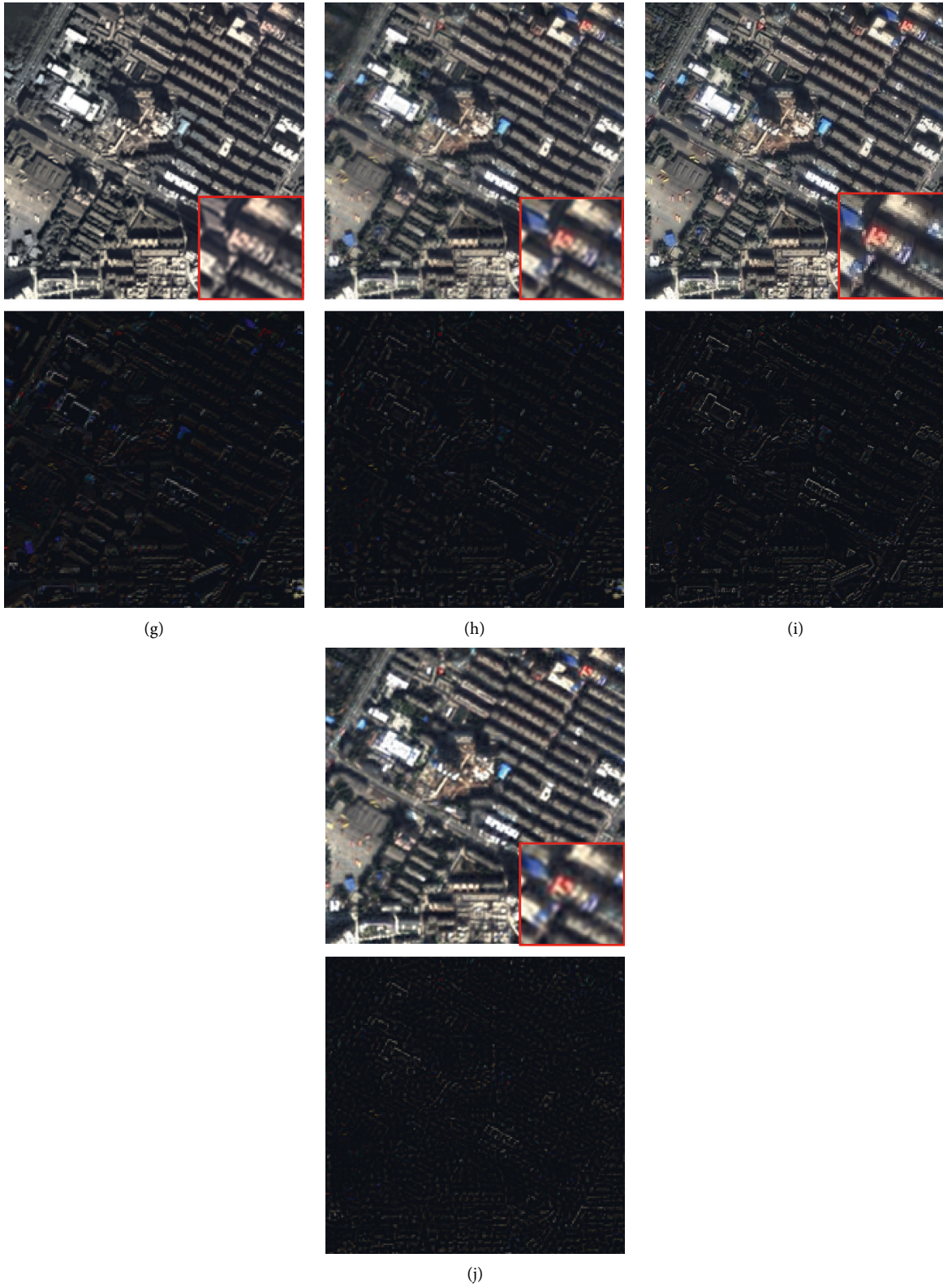
(d)

(e)

(f)

Figure 4: Continued.

FIGURE 4: The result of QuickBird data. (a) MS image. (b) PAN image. (c) Reference image. (d) PCA. (e) GIHS. (f) CT. (g) PN-TSSC. (h) SparseFI. (i) NMF. (j) Proposed method.

TABLE 2: The indexes of Figure 4.

Metric	PCA	GIHS	CT	PN-TSSC	SparseFI	NMF	Proposed method
CC	0.9236	0.9281	0.9215	0.9062	0.9458	0.9477	**0.9493**
UIQI	0.7611	0.9141	0.9149	0.9059	0.9404	0.9426	**0.9486**
RMSE	0.1306	0.0894	0.1033	0.1009	0.0773	0.0759	**0.0742**
Q_4	0.7009	0.8380	0.8448	0.8711	0.8748	**0.8750**	0.8741
SAM	6.9335	7.3535	12.2861	8.7849	6.2622	5.8163	**5.6986**
ERGAS	4.5794	3.1702	3.6194	3.5336	2.7072	2.6579	**2.6049**

The best results is highlighted in bold.

(a)

(b)

(c)

(d)

(e)

(f)

FIGURE 5: Continued.

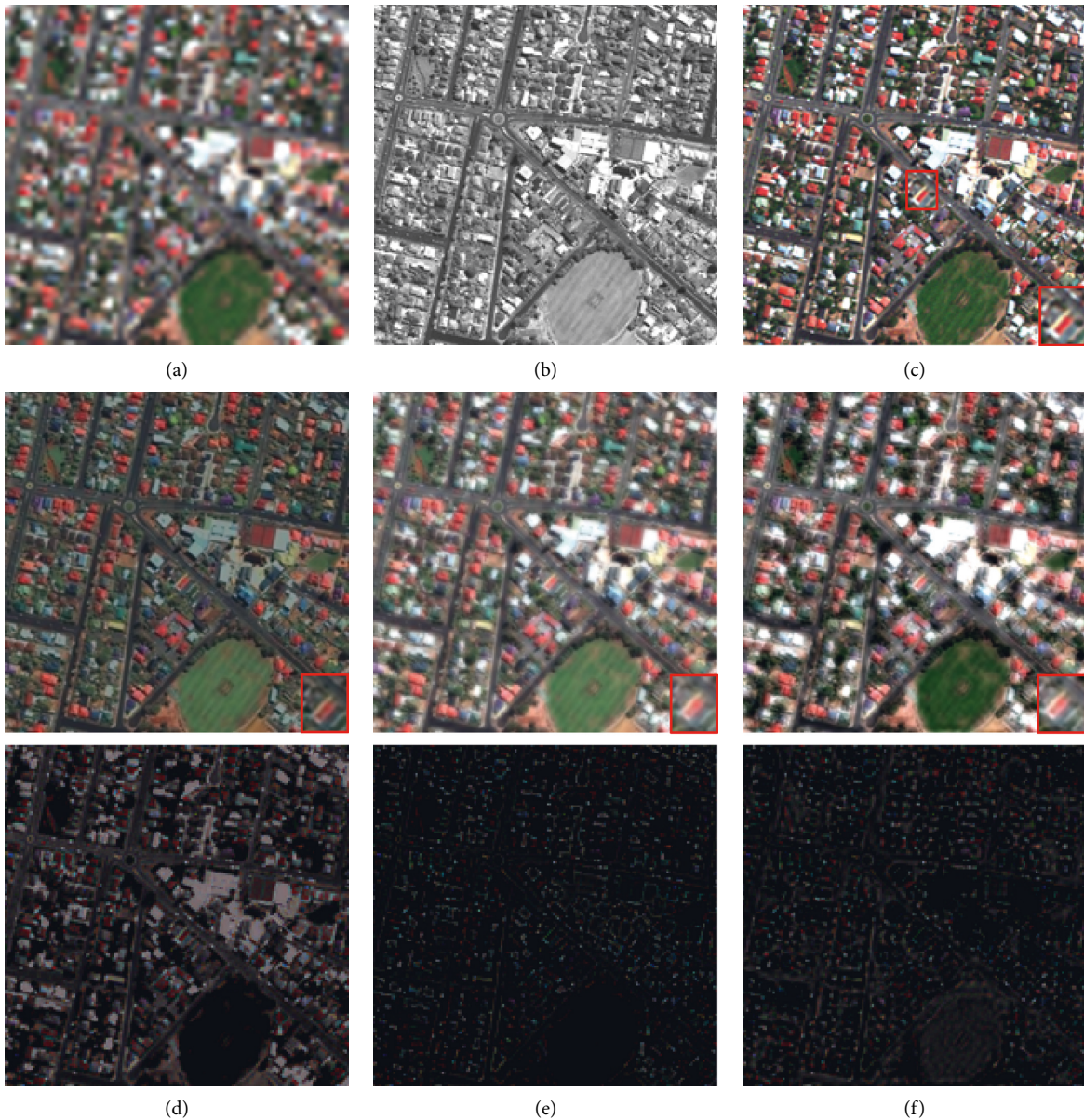(g)   (h)   (i)
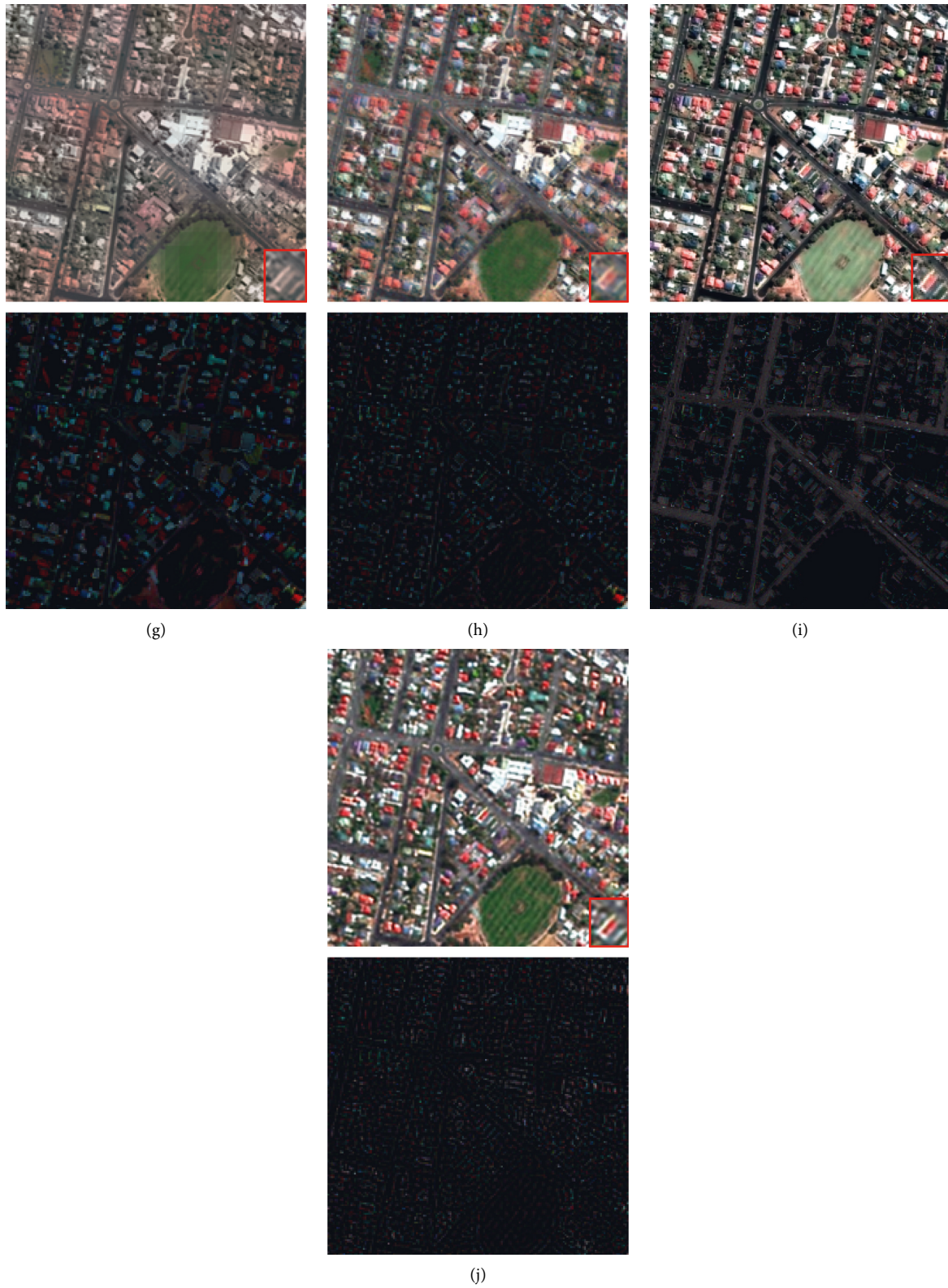

(j)

FIGURE 5: The result of GeoEye data. (a) MS image. (b) PAN image. (c) Reference image. (d) PCA. (e) GIHS. (f) CT. (g) PN-TSSC. (h) SparseFI. (i) NMF. (j) Proposed method.

TABLE 3: The indexes of Figure 5.

Metric	PCA	GIHS	CT	PN-TSSC	SparseFI	NMF	Proposed method
CC	0.8633	0.8934	0.8809	0.8448	**0.9177**	0.8584	0.9104
UIQI	0.6854	0.8574	0.8742	0.7735	0.8988	0.8508	**0.9081**
RMSE	0.1761	0.1142	0.1163	0.1329	**0.0962**	0.1316	0.0993
Q_4	0.5376	0.6421	0.6750	0.6664	0.6939	**0.7347**	0.6992
SAM	12.7007	8.1727	8.6824	12.7458	8.2269	13.7503	**7.5535**
ERGAS	5.1985	3.2027	3.2796	3.7257	2.6988	3.7984	**2.6844**

(a)

(b)

(c)

(d)

(e)

(f)

FIGURE 6: Continued.

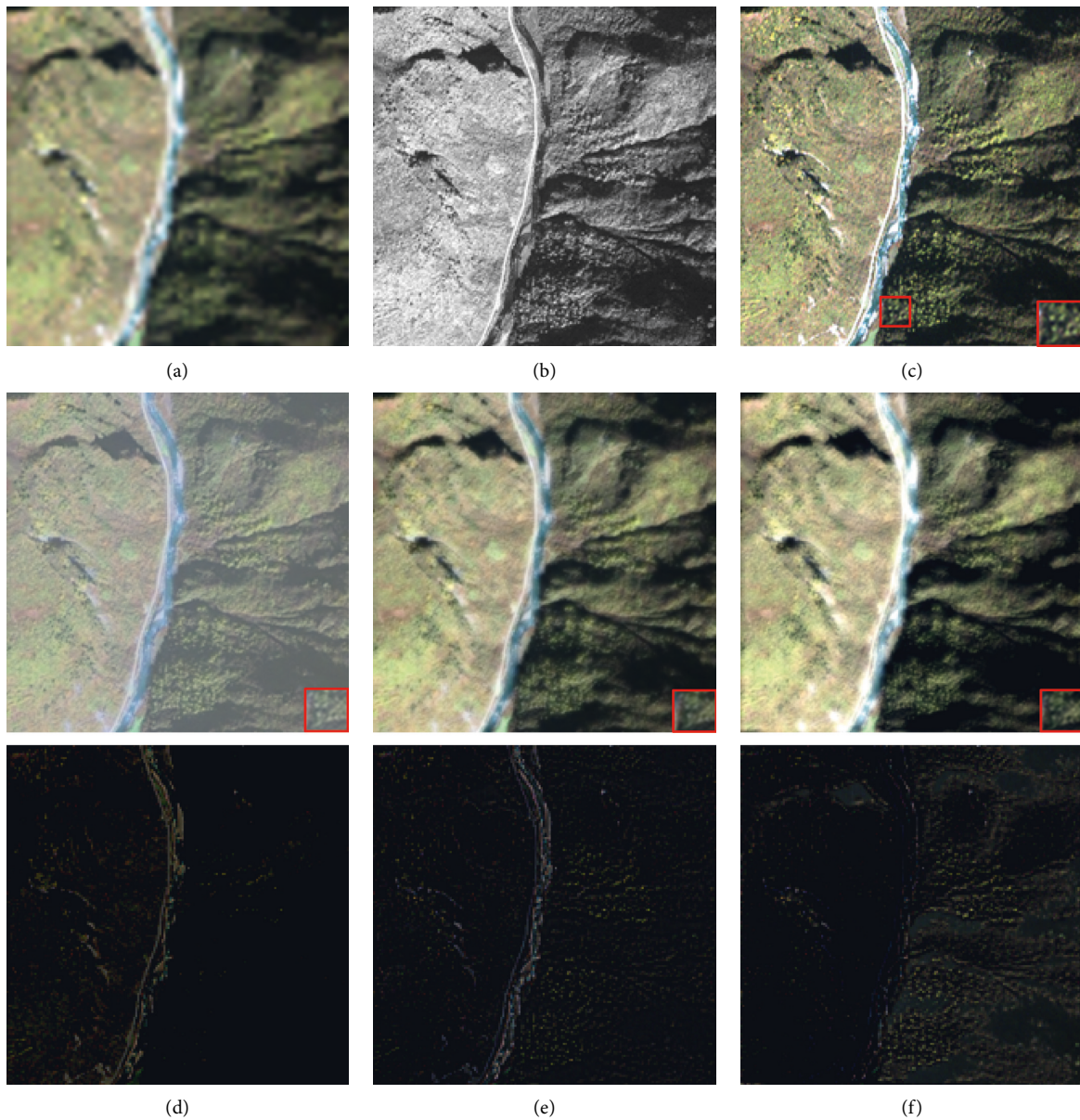(g)   (h)   (i)
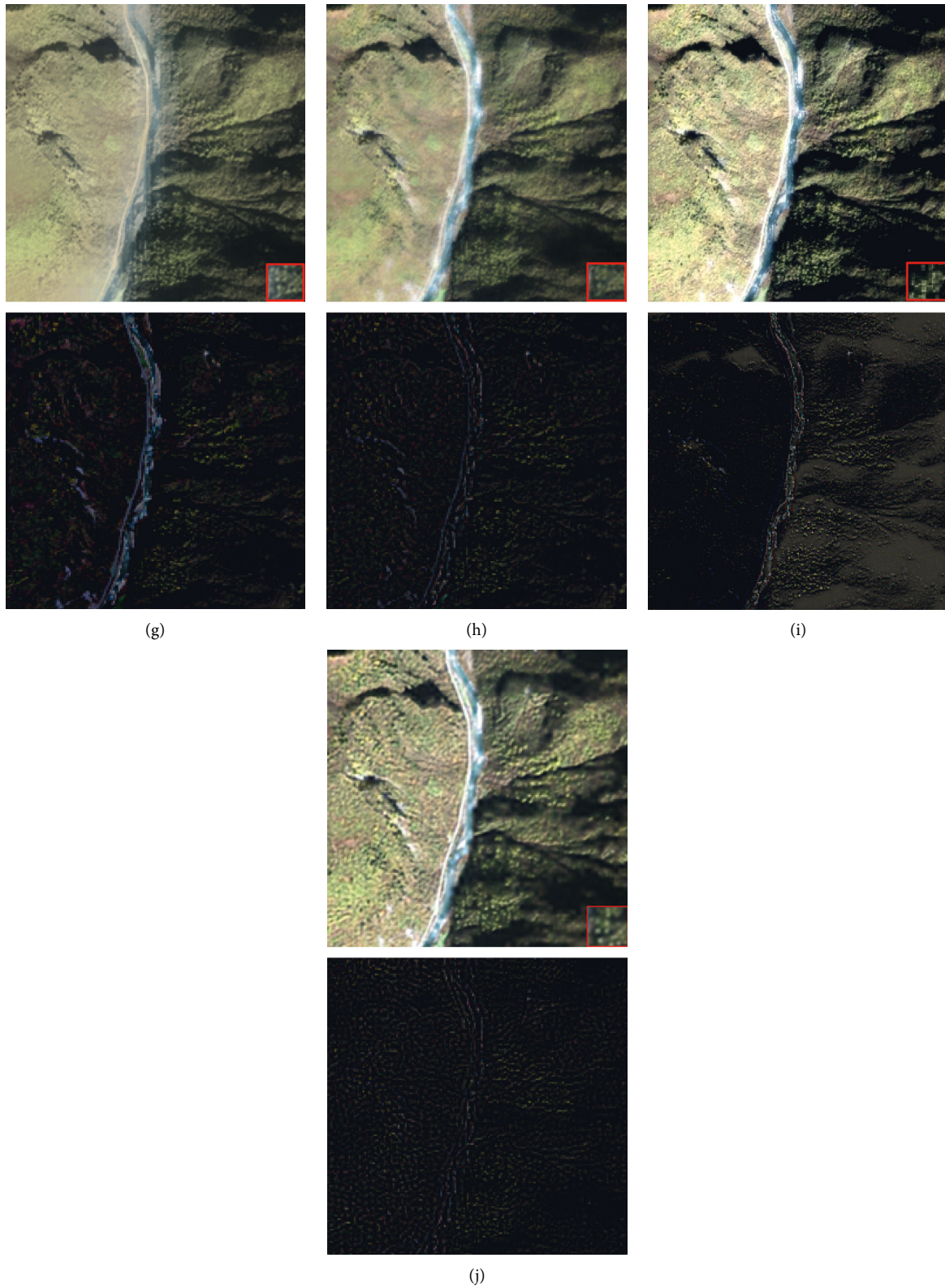

(j)

FIGURE 6: The result of IKONOS data. (a) MS image. (b) PAN image. (c) Reference image. (d) PCA. (e) GIHS. (f) CT. (g) PN-TSSC. (h) SparseFI. (i) NMF. (j) Proposed method.

TABLE 4: The indexes of Figure 6.

Metric	PCA	GIHS	CT	PN-TSSC	SparseFI	NMF	Proposed method
CC	0.9051	0.9247	0.9288	0.9041	0.9334	0.9257	**0.9364**
UIQI	0.6511	0.9222	0.9062	0.8923	0.9296	0.8848	**0.9358**
RMSE	0.2182	0.0986	0.1254	0.1092	0.0921	0.1460	**0.0903**
Q_4	0.4251	0.6395	0.6157	0.5914	0.6414	0.6245	**0.6910**
SAM	9.0099	8.0188	24.1547	8.2061	7.3057	**9.9468**	7.1104
ERGAS	6.7769	2.9956	3.8000	3.3304	2.7934	4.4245	**2.7362**

The best results are highlighted in bold.

area of the PN-TSSC method, the color information is lost seriously. In the SparseFI, NMF, and proposed method, the spatial information is close to the ground truth. However, the spectral improvements achievable can be easily remarked for our method. Table 2 shows the numerical values of fusion results. We can see that the best Q_4 is obtained from the NMF method, and the MDTR method provides the best CC, UIQI, RMSE, SAM, and ERGAS.

4.2. GeoEye Dataset. The fused results of GeoEye dataset is exhibited in this portion. The PAN image is 0.5 m resolution. The MS image is 2.0 m resolution. Figure 5 shows the result of different measures. Figures 5(a)–5(b) are MS and PAN images, respectively. Figure 5(c) is the reference MS image. In addition, we analyze the difference image. In Figure 5(d), we can see that the spatial details preserve well, but the result is darkness. In Figures 5(e) and 5(f), there are slight spectral distortion and ringing artifacts. In Figure 5(g), the color information is poor. In Figures 5(h) and 5(i), the spatial details are enhanced although the spectral information is slight distortion. From the visual effect, the result from the MDTR method is close to the ground truth, and the missing information is less. Meanwhile, we can see that the difference image information of MDTR method is less than that of other compared methods.

Table 3 shows the results of each assessment indexes. The best UIQI, SAM, and ERGAS are given by the MDTR method. For CC and RMSE, the best values are produced by SparseFI, and the best Q_4 performs the NMF method.

4.3. IKONOS Dataset. In this section, IKONOS dataset are tested. IKONOS dataset is 1 m resolution and 4 m resolution in PAN and MS images, respectively. The fused result is shown in Figures 6(d)–6(j). The enlarged area in the red rectangles appears in the fused result, and the difference image is illustrated in the second row. All the fusion images provide enhanced spatial information. But the result is darkness for the PCA method. For GIHS, CT, PN-TSSC, and NMF methods, fused images has inferior performance in terms of the spatial information. For the proposed method, spatial details are maintained well, and the fused image is close to the reference image. For the enlarged region, the fused image of the MDTR method is better than the other fused images. From Table 4, the best SAM is from the NMF method. Other best indexes are from the MDTR method.

5. Conclusions

In this paper, we propose a new pansharpening with the multidirection tree ridgelet dictionary. Our method is assessed on three datasets. The contribution of our work is to construct the multidirection tree ridgelet dictionary, which can capture the different directional information of blocks. The spatial and spectral quality of the fused image is evaluated by six different indexes. Experimental results show that our proposed method can supress the color distortions in the fused image. Meanwhile, our method can produce satisfactory performance in both visual comparison and numerical evaluations. The future work will perform DNN and tensor-based methods to explore the spatial information and maintain image spatial relationships.

Data Availability

The datasets were obtained from the website https://resources.maxar.com/.

Conflicts of Interest

The authors declare that they have no conflicts of interest.

Acknowledgments

References

[1] P. Liu and L. Xiao, "Multicomponent driven consistency priors for simultaneous decomposition and pansharpening," *IEEE Journal of Selected Topics in Applied Earth Observations and Remote Sensing*, vol. 12, no. 11, pp. 4589–4605, 2019.
[2] P. S. Chavez, S. C. Sides, and J. A. Anderson, "Comparison of three different methods to merge multiresolution and

multispectral data: landsat TM and SPOT Panchromatic," *Photogrammetric Engineering & Remote Sensing*, vol. 57, no. 3, pp. 295–303, Mar. 1991.

[3] T. M. Tu, P. S. Huang, C. L. Hung, and C. P. Chang, "A fast Intensity-Hue-Saturation fusion technique with spectral adjustment for IKONOS imagery," *IEEE Geoscience and Remote Sensing Letters*, vol. 1, no. 4, pp. 309–312, Oct. 2004.

[4] M. Myungjin Choi, "A new Intensity-Hue-Saturation fusion approach to image fusion with a tradeoff parameter," *IEEE Transactions on Geoscience and Remote Sensing*, vol. 44, no. 6, pp. 1672–1682, 2006.

[5] V. P. Shah, N. H. Younan, and R. King, "Pan-sharpening via the contourlet transform," in *Proceedings of the. IEEE Int. Symp. Geosci. Remote Sens*, pp. 310–313, IGARSS), Spain, 2007.

[6] Y. Xing, M. Wang, S. Yang, and K. Zhang, "Pansharpening with multiscale geometric support tensor machine," *IEEE Transactions on Geoscience and Remote Sensing*, vol. 56, no. 5, pp. 2503–2517, May 2018.

[7] S. Li and B. Yang, "A new pan-sharpening method using a compressed sensing technique," *IEEE Transactions on Geoscience and Remote Sensing*, vol. 49, no. 2, pp. 738–746, Feb. 2011.

[8] X. X. Zhu and R. Bamler, "A sparse image fusion algorithm with application to pan-sharpening," *IEEE Transactions on Geoscience and Remote Sensing*, vol. 51, no. 5, pp. 2827–2836, 2013.

[9] C. Jiang, H. Zhang, H. Shen, and L. Zhang, "Two-step sparse coding for the pan-sharpening of remote sensing images," *IEEE Journal of Selected Topics in Applied Earth Observations and Remote Sensing*, vol. 7, no. 5, pp. 1792–1805, 2014.

[10] M. Guo, H. Zhang, J. Li, L. Zhang, and H. Shen, "An online coupled dictionary learning approach for remote sensing image fusion," *IEEE Journal of Selected Topics in Applied Earth Observations and Remote Sensing*, vol. 7, no. 4, pp. 1284–1294, 2014.

[11] W. Wang, L. Jiao, S. Yang, and K. Rong, "Distributed compressed sensing-based pan-sharpening with hybrid dictionary," *Neurocomputing*, vol. 155, pp. 320–333, May. 2015.

[12] H. Li, F. Liu, S. Yang, K. Zhang, X. Su, and L. Jiao, "Refined pan-sharpening with NSCT and hierarchical sparse autoencoder," *IEEE Journal of Selected Topics in Applied Earth Observations and Remote Sensing*, vol. 9, no. 12, pp. 5715–5725, 2016.

[13] K. Zhang, F. Zhang, Z. X. Feng, J. D. Sun, and Q. Y. Wu, "Fusion of panchromatic and multispectral images using multiscale convolution sparse decomposition," *IEEE Journal of Selected Topics in Applied Earth Observations and Remote Sensing*, vol. 14, no. 1, pp. 426–439, Jan. 2021.

[14] H. Li, F. Wu, and X. Zhang, "Fusion of multispectral and panchromatic images via local geometrical similarity," *Tehnički Vjesnik - Tehnical Gazette*, vol. 25, no. 2, pp. 546–552, Apr. 2018.

[15] H. Yin, "PAN-guided cross-resolution projection for local adaptive sparse representation- based pansharpening," *IEEE Transactions on Geoscience and Remote Sensing*, vol. 57, no. 7, pp. 4938–4950, 2019.

[16] K. Zhang, F. Zhang, and S. Yang, "Fusion of multispectral and panchromatic images via spatial weighted neighbor embedding," *Remote Sensing*, vol. 11, no. 5, pp. 557–575, Mar. 2019.

[17] H. Li, W. Li, and S. Liu, "Pansharpening with support vector transform and semi-nonnegative matrix factorization," *Multimedia Tools and Applications*, vol. 78, no. 6, pp. 7563–7578, 2019.

[18] Z. Shao and J. Cai, "Remote sensing image fusion with deep convolutional neural network," *IEEE Journal of Selected Topics in Applied Earth Observations and Remote Sensing*, vol. 11, no. 5, pp. 1656–1669, May 2018.

[19] J. Ma, W. Yu, C. Chen, P. Liang, X. Guo, and J. Jiang, "PanGAN: an unsupervised pan-sharpening method for remote sensing image fusion," *Information Fusion*, vol. 62, pp. 110–120, Oct. 2020.

[20] K. Zhang, A. Wang, F. Zhang, W. Diao, J. Sun, and L. Bruzzone, "Spatial and spectral extraction network with adaptive feature fusion for pansharpening," *IEEE Transactions on Geoscience and Remote Sensing*, vol. 60, pp. 1–14, 2022.

[21] D. Lei, H. Chen, L. Zhang, and W. Li, "NLRNet: an efficient nonlocal attention resnet for pansharpening," *IEEE Transactions on Geoscience and Remote Sensing*, vol. 60, no. 3, pp. 1–13, 2022.

[22] M. Aharon, M. Elad, and A. Bruckstein, "K-SVD: an algorithm for designing overcomplete dictionaries for sparse representation," *IEEE Transactions on Signal Processing*, vol. 54, no. 11, pp. 4311–4322, 2006.

[23] L. Lin, F. Liu, and L. Jiao, "Compressed sensing by collaborative reconstruction on overcomplete dictionary," *Signal Processing*, vol. 103, pp. 92–102, 2014.

[24] L. Alparone, L. Wald, J. Chanussot, C. Thomas, P. Gamba, and L. M. Bruce, "Comparison of pansharpening algorithms: outcome of the 2006 GRS-S data-fusion contest," *IEEE Transactions on Geoscience and Remote Sensing*, vol. 45, no. 10, pp. 3012–3021, 2007.

[25] Z. Wang and A. C. Bovik, "A universal image quality index," *IEEE Signal Processing Letters*, vol. 9, no. 3, pp. 81–84, Mar. 2002.

[26] L. Alparone, S. Baronti, A. Garzelli, and F. Nencini, "A global quality measurement of pan-sharpened multispectral imagery," *IEEE Geoscience and Remote Sensing Letters*, vol. 1, no. 4, pp. 313–317, Oct. 2004.